arXiv:cond-mat/0608168v1 [cond-mat.mtrl-sci] 7 Aug 2006

Electronic structure of normal and inverse spinel ferrites from first principles

Z. Szotek[1], W.M. Temmerman[1], D. Ködderitzsch[2], A. Svane[3], L. Petit[4], and H. Winter[5]
[1] *Daresbury Laboratory, Daresbury, Warrington, WA4 4AD, Cheshire, U.K.*
[2] *Physikalische Chemie, Ludwig-Maximilian University, Munich, Germany*
[3] *Department of Physics and Astronomy, University of Aarhus, DK-8000 Aarhus C, Denmark*
[4] *Computer Science and Mathematics Division, and Center for Computational Sciences, Oak Ridge National Laboratory, Oak Ridge, TN 37831, USA*
[5] *IFP, Forschungszentrum Karlsruhe GmbH, Postfach 3640, D-76021 Karlsruhe, Germany*
(Dated: February 6, 2008)

We apply the self-interaction corrected local spin density approximation to study the electronic structure and magnetic properties of the spinel ferrites $MnFe_2O_4$, Fe_3O_4, $CoFe_2O_4$, and $NiFe_2O_4$. We concentrate on establishing the nominal valence of the transition metal elements and the ground state structure, based on the study of various valence scenarios for both the inverse and normal spinel structures for all the systems. For both structures we find all the studied compounds to be insulating, but with smaller gaps in the normal spinel scenario. On the contrary, the calculated spin magnetic moments and the exchange splitting of the conduction bands are seen to increase dramatically when moving from the inverse spinel structure to the normal spinel kind. We find substantial orbital moments for $NiFe_2O_4$ and $CoFe_2O_4$.

I. INTRODUCTION

The field of spintronics is concerned with search for highly spin-polarized materials. One aim is to enhance tunnelling magnetoresistance (TMR) of magnetic tunnel junctions (MTJs) which are active members of magnetic random access memory (MRAM) elements. Also, the highly spin-polarized materials are of paramount importance for increasing spin-polarization of currents injected into semiconductors, required for an optimal operation of spintronics devices.[1] There appears to be a number of ways to achieve high spin-polarization, most notably by employing fully spin-polarized ferromagnetic metals, namely half-metals (HM).[2] Another possibility is to exploit features of the band structure of such tunnel barrier materials as e.g. MgO, and filtering electronic wave functions according to their symmetry in order to select the most highly spin-polarized ones.[3,4] The least explored possibility is exploiting the spin-filtering effect, based on ferromagnetic or ferrimagnetic insulating barriers. It was introduced by Moodera et al.[5], using EuS tunnel barriers. Spin filtering effect has been demonstrated in Gd/EuS/Al junctions[6], which exhibit high magnetoresistance, but show no great prospects for technological applications, on account of the low Curie temperature, T_c, of EuS.

Spinel ferrites[7] have been studied for many years both regarding their magnetic behaviour and correlated nature in conjunction with their structural properties to increase their performance in high-frequency devices. Some of them can probably be used as spin filters. Spin-dependent gap should result in spin-dependent barrier for tunnelling of electrons through the insulator, giving rise to spin filtering. Since the tunnelling probability depends exponentially on the barrier height, the spin filtering efficiency can be very high. Candidates for spin filters include such spinel ferrites as $NiFe_2O_4$, $CoFe_2O_4$ and $MnFe_2O_4$[8]. In particular, recently a spin filtering efficiency of up to 22% by the $NiFe_2O_4$ barrier has been reported by Lüders et al.[9,10] In addition, Lüders et al.[11,12] have demonstrated TMR of 120% in $La_{2/3}Sr_{1/3}MnO_3/SrTiO_3/NiFe_2O_4$ junctions, which corresponds to 45% spin polarization for the conductive $NiFe_2O_4$ film, which stays constant up to about 300 K.

These spinel ferrites belong to the same family as magnetite (Fe_3O_4) which has been most thoroughly studied both for its HM character and the famous charge order[13,14]. Many theoretical studies have been dedicated to magnetite, and in particular its charge order (which will not be discussed in the present paper) using various approximations to density functional theory (DFT) such as local spin density (LSD) approximation or generalized gradient approximation (GGA), as well as going beyond, for example by invoking the Hubbard U through the LDA+U (local density approximation + U) approach, or using the self-interaction corrected (SIC)-LSD method.[15,16,17,18,19,20] For the other spinel ferrites most theoretical studies have been done with LSD, GGA[8,21,22,23] or hybrid density functionals.[24] The former two approaches usually describe these materials to be half-metallic and not insulating, if no distortions are included. The reason is that the transition metal (TM) d electrons in oxides (as well as f electrons in rare earth compounds) are strongly correlated and cannot be adequately described within the standard band theory framework with such approximations as LSD or GGA, placing them too high in energy around the Fermi level. The SIC-LSD method[25], on the other hand, provides better description of correlations than LSD, and was successfully applied to a variety of $d-$ and $f-$electron materials[26,27,28]. In this paper we apply the self-interaction corrected local spin density (SIC-LSD) approximation to study the electronic structure of spinel transition metal oxides $MnFe_2O_4$, Fe_3O_4, $CoFe_2O_4$, and $NiFe_2O_4$. We concentrate on the nominal valence of the TM elements and electronic and magnetic properties of

these systems in both normal and inverse spinel structures. The reason being that in most cases these materials appear to exist as some mixture of those structures.

The paper is organized as follows. An overview of the basic features of the SIC-LSD formalism is presented in the next section. Section III gives some computational details, whilst the results of the application of the SIC-LSD method to the spinel ferrites $TMFe_2O_4$ (with TM=Mn, Fe, Co and Ni), are presented and discussed in section IV. The paper is concluded in section V.

II. THEORY

The basis of the SIC-LSD formalism is a self-interaction free total energy functional, E^{SIC}, obtained by subtracting from the LSD total energy functional, E^{LSD}, a spurious self-interaction of each occupied electron state ψ_α[29], namely

$$E^{SIC} = E^{LSD} - \sum_{\alpha}^{occ.} \delta_\alpha^{SIC}. \quad (1)$$

Here α numbers the occupied states and the self-interaction correction for the state α is

$$\delta_\alpha^{SIC} = U[n_\alpha] + E_{xc}^{LSD}[\bar{n}_\alpha], \quad (2)$$

with $U[n_\alpha]$ being the Hartree energy and $E_{xc}^{LSD}[\bar{n}_\alpha]$ the LSD exchange-correlation energy for the corresponding charge density n_α and spin density $\bar{n}_\alpha$. It is the LSD approximation to the exact exchange-correlation energy functional which gives rise to the spurious self-interaction. The exact exchange-correlation energy E_{xc} has the property that for any single electron spin density, $\bar{n}_\alpha$, it cancels exactly the Hartree energy, thus

$$U[n_\alpha] + E_{xc}[\bar{n}_\alpha] = 0. \quad (3)$$

In the LSD approximation this cancellation does not take place, and for well localized states the above sum can be substantially different than zero. For extended states in periodic solids the self-interaction vanishes.

The SIC-LSD approach can be viewed as an extension of LSD in the sense that the self-interaction correction is only finite for spatially localized states, while for Bloch-like single-particle states E^{SIC} is equal to E^{LSD}. Thus, the LSD minimum is also a local minimum of E^{SIC}. A question now arises, whether there exist other competitive minima, corresponding to a finite number of localized states, which could benefit from the self-interaction term without loosing too much of the energy associated with band formation. This is often the case for rather well localized electrons like the $3d$ electrons in transition metal oxides or the $4f$ electrons in rare earth compounds. It follows from minimization of Eq. (1) that within the SIC-LSD approach such localized electrons move in a different potential than the delocalized valence electrons which respond to the effective LSD potential. Thus, by including an explicit energy contribution for an electron to localize, the *ab initio* SIC-LSD describes both localized and delocalized electrons on an equal footing, leading to a greatly improved description of correlation effects over the LSD approximation, as well as, to determination of valence.

In order to make the connection between valence and localization more explicit, it is useful to define the nominal valence[28] as

$$N_{val} = Z - N_{core} - N_{SIC},$$

where Z is the atomic number (26 for Fe), N_{core} is the number of core (and semi-core) electrons (18 for Fe), and N_{SIC} is the number of localized, i.e., self-interaction corrected, states (either five or six, respectively for Fe^{3+} and Fe^{2+}). Thus, in this formulation the valence is equal to the integer number of electrons available for band formation. The localized electrons do not participate in bonding. To find the nominal valence we assume various atomic configurations, consisting of different numbers of localized states, and minimize the SIC-LSD energy functional of Eq. (1) with respect to the number of localized electrons.

The SIC-LSD formalism is governed by the energetics due to the fact that for each orbital the SIC differentiates between the energy gain due to hybridization of the orbital with the valence bands and the energy gain upon localization of the orbital. Whichever wins determines if the orbital is part of the valence band or not, and in this manner also leads to the evaluation of the valence of elements involved. The SIC depends on the choice of orbitals and its value can differ substantially as a result of this. Therefore, one has to be guided by the energetics in defining the most optimally localized orbitals to determine the absolute energy minimum of the SIC-LSD energy functional. The advantage of the SIC-LSD formalism is that for such systems as transition metal oxides or rare earth compounds the lowest energy solution will describe the situation where some single-electron states may not be of Bloch-like form. Specifically, in oxides, Mn-, Co-, Ni-, and Fe-$3d$ states may be assumed to be localized, but not the O $2p$ states, because treating them as localized is energetically unfavourable.

The SIC-LSD approach has been implemented[25] within the linear muffin-tin-orbital (LMTO) atomic sphere approximation (ASA) band structure method[30], in the tight-binding representation[31]. In this method the polyhedral Wigner Seitz cell is approximated by slightly overlapping atom centered spheres, with a total volume equal to the actual crystal volume, while the electron wave functions are expanded in terms of the screened muffin-tin orbitals, and the minimization of E^{SIC} becomes non-linear in the expansion coefficients. The so-called combined correction term[32] has been implemented and consistently applied to improve on the ASA.

TABLE I: The lattice constants (a) and corresponding ASA radii (r_{ASA}) for the transition metal elements occupying tetrahedral (*tet*) and octahedral (*oct*) sites, and for oxygen ions (in atomic units) for all the studied spinel ferrites. The radii of the empty spheres used in the calculations are not given, although typically four to five different types were used, all of the order of 1.65 - 1.95 atomic units, depending on the system, however, never exceeding the size of the oxygen spheres.

System	a	${r_{ASA}}^{tet}$	${r_{ASA}}^{oct}$	${r_{ASA}}^{O1}$	${r_{ASA}}^{O2}$
$MnFe_2O_4$	16.08	2.204	2.588	1.979	1.979
Fe_3O_4	15.87	2.329	2.752	1.848	1.848
$CoFe_2O_4$	15.84	2.434	2.696	1.928	1.928
$NiFe_2O_4$	15.78	2.425	2.686	1.920	1.920

III. COMPUTATIONAL DETAILS

The spinel ferrites of interest to the present study have a general chemical formula of the form AB_2O_4 and crystallize in the face-centred cubic structure. In the normal spinel structure A is a divalent element atom, occupying tetrahedral A sites, while B is a trivalent element, sitting on the octahedral B sites. When A is a trivalent element, and B consists of equal numbers of divalent and trivalent elements, distributed over crystalographically equivalent B1 and B2 octahedral sites, then the spinel structure is referred to as the inverse kind. In TM ferrites substantial off-stoichiometry and intersite disorder are often present in samples, but are not considered in this paper. The high temperature phase of magnetite is known to have the inverse spinel structure, where A atoms are Fe^{3+} ions, and B sites are equally populated by Fe^{2+} and Fe^{3+} ions. Similarly, the $NiFe_2O_4$ system has been established experimentally to crystallize in the inverse spinel structure, with the A sites being Fe^{3+} ions, while B sites equally populated by Ni^{2+} and Fe^{3+} ions. The $MnFe_2O_4$, on the other hand, is considered to be predominantly of the normal spinel kind, as about 80% of A sites are populated by Mn^{2+} ions.[7,33] The $CoFe_2O_4$ material is considered to be mostly an inverse spinel compound with about 80% of divalent Co ions occupying octahedral sites.[7,34,35] As the experimental situation with respect to the observed structures and TM valences is not fully established, and the computer simulation of the exact physical conditions is very difficult, in this paper we study both extremes, namely the normal and inverse spinel structures for all the systems. In addition, we investigate a number of different valence scenarios, defined in the following sections, to find the most energetically favourable solutions, be it only at zero temperature, for all the studied systems.

Regarding the magnetic structure of the ferrites, we assume that of magnetite, with the spins of the TM atoms on the tetrahedral sublattice being antiparallel to those of the octahedral sublattice. Within a given sublattice the spins of all the TM atoms are arranged in parallel to one another.

The calculations have been performed for the experimental lattice parameters, whose values, together with the corresponding ASA radii, are given in Table I.[8]. For the basis functions, we have used s-, p-, and d-muffin-tin orbitals on all the transition metal atoms as the so-called low waves and on the oxygen the s- and p-orbitals have been treated as low waves and the d-orbitals have been downfolded[36]. For a better space filling and to increase the number of basis functions, a set of empty spheres has also been included in the calculations. For the empty spheres only the s basis functions have been treated as low waves, while both p- and d-orbitals have been downfolded. All the calculations have been performed in the scalar-relativistic mode, but for the calculated ground state configurations the spin-orbit coupling (SOC) was also included to calculate the orbital moment, in addition to the spin moment.

IV. RESULTS AND DISCUSSION

A. $MnFe_2O_4$

As mentioned earlier, this compound is believed to be of predominantly normal spinel character. It is insulating, with a small gap of 0.04-0.06 eV as determined by transport experiments.[37] Our calculations have adressed the important issues of this system by realizing both normal ('N') and inverse ('I') spinel arrangements of ions on the tetrahedral and octahedral sites. In addition, the all 3+ scenario, where all the sites are occupied exclusively by the 3+ ions, has also been studied. Note that in the normal spinel environment the latter would mean that Mn^{3+} (four d electrons are considered as localized) ions occupy the tetrahedral sites, while all the octahedral sites are exclusively populated by Fe^{3+} ions ('N3+' scenario). For the inverse spinel environment the tetrahedral ions would be of Fe^{3+} type, with the B1 octahedral sites occuped by Mn^{3+} ions and the B2 sites by Fe^{3+} ions ('I3+' scenario). In Table II, we summarize the total energy differences for all the scenarios studied for $MnFe_2O_4$, in comparison with all the other spinel ferrites.

We find the normal spinel arrangement of ions to be the calculated ground state for $MnFe_2O_4$ (Table II), in agreement with the experimental evidence for predominantly normal spinel character of this compound. The ground state solution is followed closely by the all 3+ scenario, realized in the normal spinel environment ('N3+'), which lies only 0.28 eV higher in energy. The inverse spinel solution is 0.58 eV higher, while the 'I3+' scenario is the most unfavourable state for $MnFe_2O_4$.

To establish whether the degree of localization of d electrons of the TM ions residing on the tetrahedral sites has any bearing on the preference towards normal spinel structure in $MnFe_2O_4$, we have looked at the change in the localization energy when switching Mn^{2+} ion between the tetrahedral and octahedral sites. We have found that the localization energy associated with Mn^{2+} on the tetrahedral sites is 0.15 eV smaller than when Mn^{2+} ions

TABLE II: Total energy differences (in eV per formula unit), calculated within SIC-LSD, between the ground state configuration and other valence/structure scenarios for all studied spinel ferrites at the experimental lattice constant. The row marked by 'N' means normal spinel arrangement, where the tetrahedral sites are occupied by the divalent ions, namely Mn^{2+} in $MnFe_2O_4$ compound, Fe^{2+} in Fe_3O_4, Co^{2+} in $CoFe_2O_4$ and finally Ni^{2+} in $NiFe_2O_4$, while the octahedral sites are populated exclusively by Fe^{3+} ions. Similarly, the row marked by 'I' means that the B1 sites are occupied by Mn^{2+} in $MnFe_2O_4$, Fe^{2+} in Fe_3O_4, Co^{2+} in $CoFe_2O_4$ and Ni^{2+} in $NiFe_2O_4$, with all the tetrahedral and B2 octahedral sites taken by the Fe^{3+} ions. The notation 'I3+' means that tetrahedral sites and B2 octahedral sites in all the compounds are occupied by Fe^{3+} ions, while the B1 octahedral sites are populated by Mn^{3+} ions in $MnFe_2O_4$, Fe^{3+} ions in Fe_3O_4, Co^{3+} ions in $CoFe_2O_4$, and Ni^{3+} ions in $NiFe_2O_4$. In the 'N3+' scenario all the octahedral sites, in all the compounds studied, are occupied by the Fe^{3+} ions, and the tetrahedral sites are taken by Mn^{3+} ions in $MnFe_2O_4$, Fe^{3+} ions in Fe_3O_4, Co^{3+} ions in $CoFe_2O_4$, and Ni^{3+} ions in $NiFe_2O_4$. Note, that in the Fe_3O_4 case the latter two scenarios, namely 'N3+' and 'I3+', are equivalent.

Scenario	$MnFe_2O_4$	Fe_3O_4	$CoFe_2O_4$	$NiFe_2O_4$
I	0.58	1.54	0.20	0.00
I3+	0.92	0.00	0.00	0.52
N	0.00	2.46	1.09	1.66
N3+	0.28	0.00	0.46	1.57

occupy the octahedral sites. At the same time the localization energy associated with the Fe^{3+} ions is smaller by 0.19 eV for the tetrahedral sites, in comparison with the situation when on the octahedral sites. Hence, the localization energy alone favours the normal spinel structure only by 0.04 eV over the inverse spinel kind, which constitutes just a tiny fraction of the total energy difference of 0.58 eV (Table II). Thus, the preference of $MnFe_2O_4$ for the normal spinel structure is mostly driven by other electronic degrees of freedom.

Regarding the density of states (DOS) of $MnFe_2O_4$ in the calculated ground state normal spinel structure (the top panel of Fig. 1), one can see that it is insulating, with a gap of about 0.075 eV which is slightly larger than the experimental value obtained from transport measurements. A larger gap of about 0.3 eV is seen for the inverse spinel structure (bottom panel), but the spin splitting of the conduction band is here considerably smaller than for the ground state normal spinel scenario (Table III). In variance to the normal and inverse spinel cases, the 'N3+' scenario (middle panel) is found to be half-metallic.

For all the studied scenarios, the valence band is predominantly of the oxygen type, with a very small admixture of the TM character, and its polarization at the top of the band changes from positive to negative between the inverse and normal spinel scenarios (Table III). What also changes substantially when moving from the normal to inverse spinel scenario is the conduction band

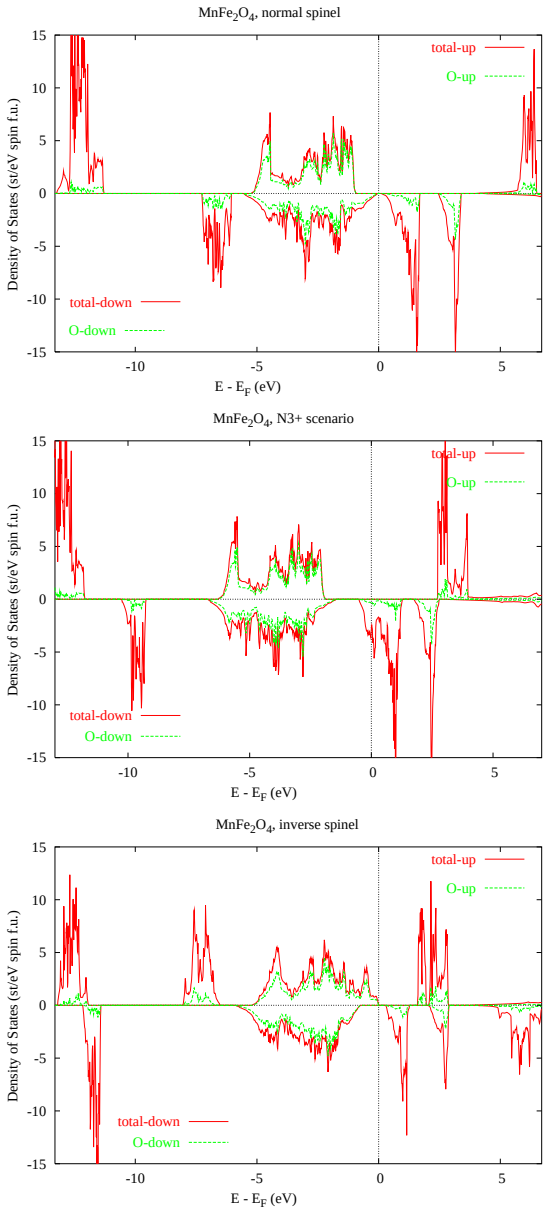

FIG. 1: (Color online) Spin decomposed total densities of states (in red), per formula unit, for $MnFe_2O_4$ for the normal spinel structure ('N') (top), for the all 3+ scenario in the normal spinel arrangement of atoms ('N3+') (middle), and for the inverse spinel scenario ('I') (bottom). The oxygen contribution to the total density of states is also shown (green, dotted lines). The minority DOS is printed on the negative side of the y-axis, while the majority contributions are presented on the positive side of this axis.

splitting, which for the normal spinel scenario is about 2.5 eV larger than that of the inverse spinel case. The reason being that the unoccupied TM *d*-states are substantially pushed up in energy when in the normal spinel environment. Considering that in reality $MnFe_2O_4$ is not a pure normal spinel compound, the exchange splitting of the conduction bands is most likely to be somewhere

TABLE III: Spin decomposed exchange splittings of the valence and conduction bands, as well as the energy gaps (in eV), for both inverse and normal spinel structures for $MnFe_2O_4$. Here VBM stands for the valence band maximum and CBM for the conduction band minimum, and ↑ refers to spin-up- and ↓ to spin-down-component.

	'I' scenario	'N' scenario
$VBM^{\uparrow}$ - $VBM^{\downarrow}$	0.69	-0.91
$CBM^{\uparrow}$ - $CBM^{\downarrow}$	1.31	3.85
$CBM^{\uparrow}$ - $VBM^{\uparrow}$	1.64	4.84
$CBM^{\downarrow}$ - $VBM^{\downarrow}$	1.02	0.075
Gap	0.33	0.075

in between the values calculated for the normal and inverse spinel scenarios. Of course, the larger the splitting, the more advantageous should it be for the spin filtering properties.

To understand details of the densities of states shown in Fig. 1, associated with the localized TM states, one should keep in mind that in the normal spinel scenario (top panel) which, as already mentioned, is the calculated ground state structure for this compound, the tetrahedral sublattice is populated by Mn^{2+} ions and that in this case five minority Mn d electrons are described as localized states, seen just below the predominantly O $2p$ valence band, at about -6 eV. The unoccupied, majority Mn d electrons give rise to the states seen as peaks above the Fermi energy at about +6 eV. The octahedral sublattice is populated by Fe^{3+} ions, with five majority d electrons localized, as the two sublattices are anti-parallel to one another. As a result the localized majority d Fe states are seen at about -12 eV below the Fermi energy. The unoccupied Fe d states, the minority ones, are seen just above the Fermi energy, over the range of up to about 3.5 eV.

In the 'N3+' scenario (middle panel), one minority Mn d electron gets delocalized to realize Mn^{3+} ions on the tetrahedral sites. As a result the localized, minority Mn d peak has moved down in energy, lying just above -10 eV, while the fifth, now delocalized, minority d electron appears at the Fermi energy, bringing down also the unoccupied, minority, Fe d states. The situation changes in the inverse spinel scenario (bottom panel), as now Mn^{2+} ions reside on B1 sites of the octahedral sublattice, while the Fe^{3+} ions populate the tetrahedral sublattice and B2 sites of the octahedral sublattice. Thus on the tetrahedral sites we have five minority Fe d electrons which give rise to the peak at about -12 eV, while the localized Fe d electrons of the octahedral sublattice are seen as the peak on the majority side, at about -14 eV. The five localized Mn majority d states are again seen just below the valence band at about -7 eV. The unoccupied Mn minority d bands are seen at about 6 eV above the Fermi energy. The five unoccupied, majority, Fe d states, associated with the tetrahedral sublattice, are seen at about 2.5 eV above the Fermi energy. Finally, the unoccupied, minority, Fe d states of the octahedral sublattice are seen as two separate peaks above the Fermi energy. Note, however, that the SIC-LSD eigenvalues have no direct physical interpretations as removal energies, and thus should not be directly compared with spectroscopies. To do so, one would need to take into account relaxation/screening effects that are not included in such an effective one-electron theory as SIC-LSD. One way to accomplish this is to employ the Δ_{SCF} calculations,[38,39,40] and another is the SIC-LSD based optimized effective potential (OEP) method.[40,43,44,45]

TABLE IV: Total spin magnetic moments (in μ_B per formula unit), calculated within SIC-LSD, for all the studied spinel ferrites and scenarios.

Scenario	$MnFe_2O_4$	Fe_3O_4	$CoFe_2O_4$	$NiFe_2O_4$
I	5.00	4.00	3.00	2.00
I3+	4.10	4.00	3.00	2.00
N	5.00	6.00	7.00	8.00
N3+	5.00	4.00	5.60	6.80

The magnetic properties change when moving from the normal to inverse spinel scenario, as seen in Table IV, where we compare the total spin magnetic moments for all the studied spinel ferrites. The total spin magnetic moment for $MnFe_2O_4$ is 5 μ_B per formula unit, for both insulating and half-metallic solutions, while for the metallic 'I3+' scenario the spin moment is reduced to 4.1 μ_B per formula unit. Note that unlike in the other ferrites there is no change in the total spin magnetic moment between the normal and inverse spinel scenarios. The reason being that, as seen in Table V, there are only very small changes in the values of the spin moments of the transition metal ions, that are compensated by changes in the induced oxygen spin moments.

TABLE V: Type-decomposed spin magnetic moments (in μ_B per formula unit), calculated within SIC-LSD, for $MnFe_2O_4$ for inverse and normal spinel structures. Here 'A' marks the tetrahedral-, while 'B1' and 'B2' the octahedral-sites, and 'O1' and 'O2' stand for two different types of oxygens.

Scenario	${Fe_A}^{3+}$	${Mn_{B1}}^{2+}$	${Fe_{B2}}^{3+}$	O1	O2
I	-4.09	4.58	4.11	0.12	0.03
Scenario	${Mn_A}^{2+}$	${Fe_{B1}}^{3+}$	${Fe_{B2}}^{3+}$	O1	O2
N	-4.49	4.11	4.11	0.34	0.34

Including spin-orbit coupling for the ground state normal spinel scenario for $MnFe_2O_4$ compound, we find no considerable orbital moments either on Mn (-0.0005 μ_B) or on Fe ions (0.019 μ_B). As a result, the total orbital moment is of the order of 0.045 μ_B per formula unit, while at the same time the total spin moment is changed from 5.0 μ_B to 4.9995 μ_B per formula unit. Also, even with SOC included, we still observe a small energy gap of 0.064 eV, which incidently is in good agreement with the transport experiments.[37]

B. Fe_3O_4

Based upon its high magnetoresistive properties, magnetite is of interest for technological applications, as e.g. computer memory, magnetic recording, etc. Magnetite is thought to be half-metallic, with the highest known T_c of 860 K. At about T_V=122 K it undergoes a transition to an insulating state, associated with some kind of charge order, setting in on the octahedral sites, and a distortion of the crystal structure from the inverse spinel cubic to monoclinic[13,14,46]. Verwey argued that below the transition temperature, T_V, the Fe^{3+} and Fe^{2+} cations order in the alternate (001) planes, and interpreted this transition as an electron localization-delocalization transition[13].

In the earlier paper, we have studied three different types of charge order on the octahedral sites, both in the high temperature (cubic) and low temperature (monoclinic) phases[20]. In this paper, for the sake of comparison with other spinel TM oxides, we concentrate exclusively on the high temperature cubic phase and the scenarios enumerated in Table IV.

As seen from Table II and Fig. 2 (middle panel), the ground state of magnetite in the cubic phase is half-metallic, with all Fe ions in 3+ configuration (five d electrons localized). This ground state scenario ('I3+'≡'N3+') is the result of a delocalization of the sixth d electron of the original Fe^{2+} ions, that together with Fe^{3+} ions randomly populate the octahedral B1 and B2 sites in the high-temperature cubic phase. In the ground state scenario, this sixth electron is seen to give rise to the peak at the Fermi energy in the minority channel, together with the other 10 unoccupied minority d states associated with the octahedral sites. The five localized tetrahedral Fe_A minority d states appear around -13 eV, while the unoccupied majority Fe_A d states are seen just above the Fermi energy. All the localized majority d states of the octahedral sites are at about -12.5 eV. The valence band is of predominantly O p character.

The inverse spinel solution (Table II and the bottom panel of Fig. 2), corresponding to the assumed Verwey charge order, lies about 1.5 eV above the ground state. In this scenario, the above mentioned sixth electron is localized on the B1-octahedral sites, and appears as a small hump at the bottom of the minority valence band. The remaining five d states of the Fe_{B1} sites are seen at about -8 eV below the Fermi energy in the majority bands. The five localized majority Fe_{B2} d states lie at about -12.5 eV. The minority Fe_A d states (seen below -10 eV) are localized, and the majority Fe_A d states are unoccupied, occuring at about 3 eV above the Fermi energy. As a result, since the four remaining minority Fe_{B1} d states and five minority Fe_{B2} states are also unoccupied, our calculations for this scenario give an insulating state with a gap of ∼0.7 eV. Understandably, as the latter has been calculated for the high-temperature inverse spinel structure, its value is much larger than the experimental value of 0.14 eV[47], measured for the true, low temperature monoclinic phase.[48]

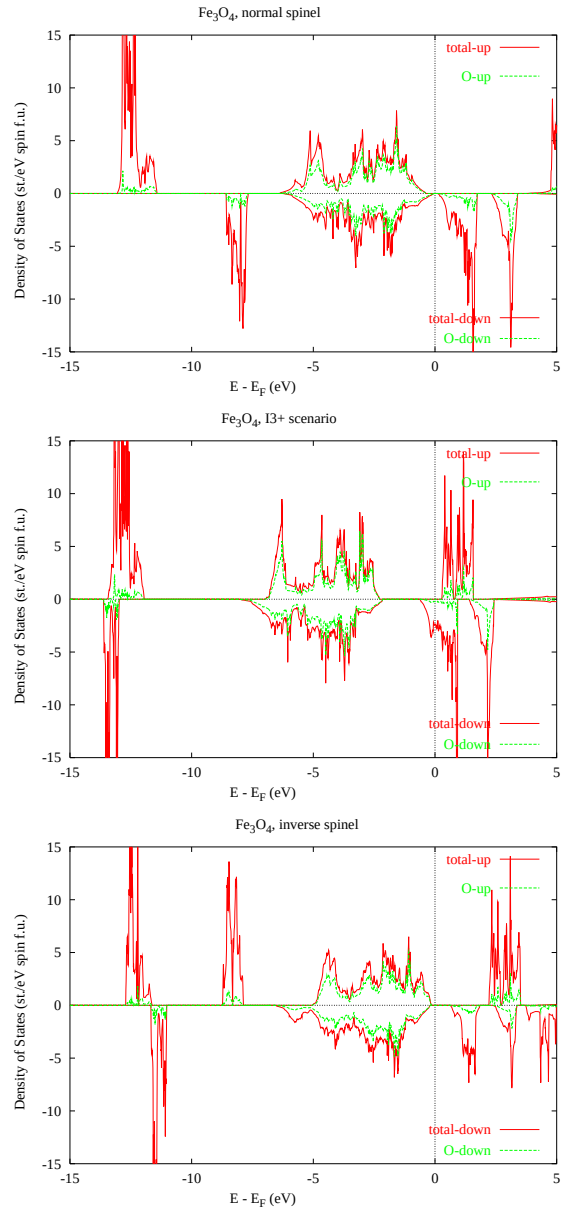

FIG. 2: (Color online) Spin decomposed total densities of states (in red), per formula unit, for Fe_3O_4 for the normal spinel structure ('N') (top), for the all 3+ scenario in the inverse spinel arrangement of atoms ('I3+') (middle), and for the inverse spinel scenario ('I') (bottom). The oxygen contribution to the total density of states is also shown (green dotted). The minority DOS is printed on the negative side of the y-axis, while the majority contribution is shown on the positive side of this axis.

Our calculations for the normal spinel structure give the most energetically unfavourable solution for magnetite, lying about 2.5 eV above the 'I3+' ground state scenario. In this normal spinel case (top panel of Fig. 2), we obtain an insulating solution with an energy gap of 0.08 eV. Here, the tetrahedral sites are occupied by Fe^{2+} ions, while the octahedral sites are populated with Fe^{3+}

TABLE VI: Spin decomposed exchange splittings of the valence and conduction bands, as well as the energy gaps (in eV), for both inverse and normal spinel structures for Fe_3O_4. Here VBM stands for the valence band maximum and CBM for the conduction band minimum, and ↑ refers to spin-up- and ↓ to spin-down-component.

	'I' scenario	'N' scenario
$VBM^{\uparrow}$ - $VBM^{\downarrow}$	0.06	-0.35
$CBM^{\uparrow}$ - $CBM^{\downarrow}$	1.61	3.65
$CBM^{\uparrow}$ - $VBM^{\uparrow}$	2.33	4.08
$CBM^{\downarrow}$ - $VBM^{\downarrow}$	0.78	0.08
Gap	0.72	0.08

TABLE VII: Total and type-decomposed spin magnetic moments (in Bohr magnetons per formula unit) for magnetite as calculated within SIC-LSD for three different scenarios. Only different Fe-types are listed in the table.

Scenario	M_{total}	$M_{Fe_A^{2+}}$	$M_{Fe_A^{3+}}$	$M_{Fe_{B1}^{2+}}$	$M_{Fe_{B1}^{3+}}$	$M_{Fe_{B2}^{3+}}$
I	4.00	-	-4.00	3.57	-	4.08
I3+	4.00	-	-4.02	-	3.90	3.90
N	6.00	-3.46	-	-	4.09	4.09

ions. As a result, five localized minority Fe_A d states lie at about -8 eV, while the sixth localized, majority, Fe_A d state sits right at the bottom of the majority valence band. All the remaining unoccupied majority Fe_A d states are just about seen at 5 eV above the Fermi energy, giving rise to a large exchange splitting of the conduction band. The localized, majority, Fe_{B1} and Fe_{B2} d states are seen at -12.5 eV, while their unoccupied, minority, states lie just above the Fermi energy, over the range of about 3-4 eV. So, again like in $MnFe_2O_4$, we see a large change in the exchange splitting of the conduction band when moving from the inverse to normal spinel structure. For the inverse spinel scenario ('I') it is of the order of 1.6 eV, while for the normal spinel arrangement it increases to 3.65 eV (Table VI). It is interesting to note, that in the normal spinel structure the sixth localized d electron of the Fe^{2+} ion occupies one of the e_g orbitals, while in the inverse spinel scenario it populates one of the t_{2g} states.

The total spin magnetic moment per formula unit is 4 μ_B (Table IV) for all the scenarios studied, with the exception of the normal spinel scenario, where we see a 50% increase to 6 μ_B. As all the scenarios give rise to either insulating or half-metallic states, the spin magnetic moments are naturally integer numbers. Table VII explains how the 50% increase in the total spin magnetic moment comes about when switching from the inverse to normal spinel structure. In the inverse spinel case the spin moment of the tetrahedral Fe ions gets just about cancelled by the spin moment of the B2-octahedral sites, so that the total spin moment is mostly due to the Fe^{2+} ions on the B1-sites. In the normal spinel, on the other hand, the spin moment of the tetrahedral Fe^{2+} ions is smaller, and oppositely alligned with the spin moments of the Fe^{3+} ions that occupy all the octahedral sites. Bearing in mind that there are twice as many octahedral sites as the tetrahedral ones, the substantial increase is easy to account for, especially that the induced spin moments on the oxygen sites do not differ much between the two scenarios.

Including spin-orbit coupling for the ground state 'I3+' scenario leads to a very small total orbital moment of about 0.05 μ_B per formula unit, while the total spin moment is very slightly reduced from 4 μ_B to 3.9998 μ_B per formula unit. The orbital moments due to the individual Fe-ions are similarly very small, with the tetrahedral Fe being -0.015 μ_B and the octahedral Fe of 0.035 μ_B.

C. $CoFe_2O_4$

This compound is believed to be mostly of the inverse spinel kind[49,50,51], with divalent Co ions occupying predominantly the octahedral sites. However, similarly to magnetite in the high temperature cubic phase, our calculations find the ground state of $CoFe_2O_4$ to be half-metallic and of the 'I3+' type (Table II and Fig. 3, middle panel). As seen in Table II, the inverse spinel scenario ('I') is not far, lying only 0.2 eV higher in energy. What this seems to imply is that this compound prefers the inverse arrangement of atoms, independently of the actual valence of the Co ions. The normal spinel solution is about 1.1 eV away. Although the ground state we find is half-metallic, the inverse spinel scenario ('I'), with Co^{2+} ions occupying the B1 octahedral positions, describes $CoFe_2O_4$ as an insulator, with a gap of 0.8 eV, which is reduced to 0.21 eV in the normal spinel case (Table VIII and Fig. 3).

To understand in detail the densities of states in Fig. 3 note that Co has only one minority electron more than Fe. So, the Co^{2+} ion has two localized minority d electrons, in addition to the five majority ones. In the ground state 'I3+' scenario (middle panel in Fig. 3), one of these two minority electrons gets delocalized, contributing to the states at the Fermi energy, while the other, localized, one is seen as a sharp peak just above -10 eV. All the remaining main features of DOS for this scenario are exactly like in the case of 'I3+' scenario in magnetite.

For the inverse spinel structure (bottom panel of Fig. 3), the situation is again very much like in magnetite (bottom panel of Fig. 2), with the exception that now we have a small double hump, at about -7 eV, slightly detached from the predominantly O $2p$ valence band, while in magnetite it was still attached to the valence band and represented just a single minority d electron.

In the normal spinel scenario the Co^{2+} ions now reside on the tetrahedral sites, with their five localized minority d states seen as a rather sharp peak at about -8 eV, in the top panel of Fig. 3. The remaining two localized majority d states are sitting just below the majority valence band. All the other features are like in magnetite.

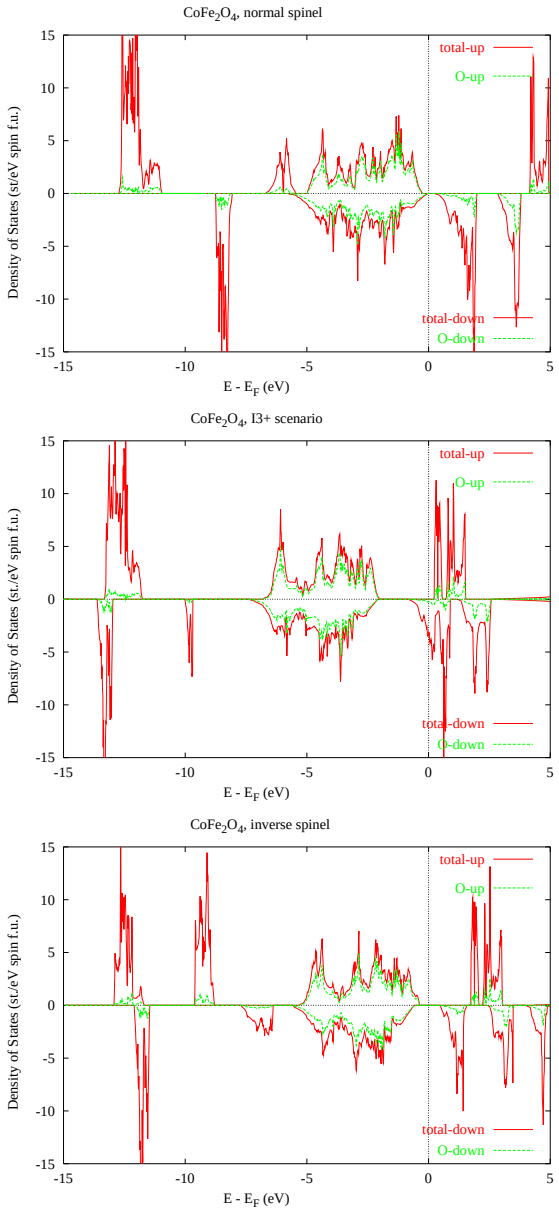

FIG. 3: (Color online) Spin decomposed total densities of states (in red), per formula unit, for $CoFe_2O_4$ for the normal spinel structure ('N') (top), for the all 3+ scenario in the inverse spinel arrangement of atoms ('I3+') (middle), and for the inverse spinel scenario ('I') (bottom). The oxygen contribution to the total density of states is also shown (green dotted lines). The minority DOS is printed on the negative side of the y-axis, while the majority contribution is shown on the positive side of this axis.

Similarly to other ferrites, one sees substantial change in the exchange splitting of the conduction band between the inverse and normal spinel scenarios, from 1.28 eV to 4.07 eV. Also, the negative spin polarization of the valence band is seen in the normal spinel, while a positive one in the inverse spinel structure. Like in magnetite, for the divalent Co^{2+} ions on the tetrahedral sites in the normal spinel structure, the e_g minority states are populated before the t_{2g} ones, which is in variance to the inverse spinel structure. In the latter case, the Co^{2+} ions reside on the B1 octahedral sites, and the t_{2g} states are lying lower in energy than the e_g states.

TABLE VIII: Spin decomposed exchange splittings of the valence and conduction bands, as well as the energy gaps (in eV), for both inverse and normal spinel structures for $CoFe_2O_4$. Here VBM stands for the valence band maximum and CBM for the conduction band minimum, and ↑ refers to spin-up- and ↓ to spin-down-component.

	'I' scenario	'N' scenario
$VBM^{\uparrow}$ - $VBM^{\downarrow}$	0.22	-0.24
$CBM^{\uparrow}$ - $CBM^{\downarrow}$	1.28	4.07
$CBM^{\uparrow}$ - $VBM^{\uparrow}$	2.08	4.52
$CBM^{\downarrow}$ - $VBM^{\downarrow}$	1.02	0.21
Gap	0.80	0.21

TABLE IX: Type-decomposed spin magnetic moments (in μ_B per formula unit), calculated within SIC-LSD, for $CoFe_2O_4$ for inverse and normal spinel scenarios. Here 'A' marks the tetrahedral-, while 'B1' and 'B2' the octahedral-sites, and 'O1' and 'O2' stand for two different types of oxygens.

Scenario	${Fe_A}^{3+}$	${Co_{B1}}^{2+}$	${Fe_{B2}}^{3+}$	O1	O2
I	-4.11	2.58	4.11	0.13	0.07
Scenario	${Co_A}^{2+}$	${Fe_{B1}}^{3+}$	${Fe_{B2}}^{3+}$	O1	O2
N	-2.58	4.13	4.13	0.32	0.32

As seen in Table IV, the total spin magnetic moment for both the 'I' and 'I3+' scenarios is 3 μ_B per formula unit. It is reduced from 4 μ_B in magnetite due to the smaller value of the spin moment of the divalent Co-ion of 2.58 μ_B (Table IX), in comparison with the spin moment of the divalent Fe ions of 3.57 μ_B (Table VII). What is however more dramatic is the change of the spin moment when moving from the inverse to the normal spinel arrangement of ions. Table IV shows that in the normal spinel scenario the total spin moment is 7 μ_B per formula unit, which again is due to the fact that the octahedral sites are populated exclusively by Fe^{3+} ions, whose spin moments are arranged in parallel to one another and whose magnitudes are considerably larger than the moment of Co^{2+} ions on the tetrahedral sites.

With respect to spin-orbit coupling we find the total orbital moment of the ground state 'I3+' scenario to be quite substantial of the order of 0.58 μ_B per formula unit, and associated mostly with the Co^{3+} ion. As the total spin moment is reduced from 3 μ_B to 2.9997 μ_B per formula unit, the ratio of the total orbital to spin moment is 0.19. The ratio of the orbital to spin moment for the Co^{3+} ion itself is 0.21.

D. $NiFe_2O_4$

$NiFe_2O_4$ is a ferromagnetic insulator that is of possible interest as a spin filter in MTJs[9,10]. This compound has the Curie temperature of 850 K, and hence has a great potential for technological applications.

In agreement with experiments, we find the ground state of $NiFe_2O_4$ to be insulating and of the inverse spinel kind (Table IV and the bottom panel of Fig. 4). The calculated energy gap is 0.98 eV (Table X). It gets reduced to 0.26 eV in the normal spinel scenario, which is the most energetically unfavourable solution for this compound. In the ground state 'I' scenario, the octahedral B1-sites are occupied by Ni^{2+} and B2 sites by Fe^{3+} ions, while the tetrahedral sites are populated exclusively by Fe^{3+} ions. Replacing the Co^{2+} ions on the octahedral sites in $CoFe_2O_4$ by Ni^{2+} leads to the reduction of the total spin magnetic moment of 3 μ_B in $CoFe_2O_4$ to 2 μ_B in $NiFe_2O_4$ (Table IV), since the spin magnetic moment of the Ni^{2+} ion is 1.57 μ_B (Table XI), as compared to 2.58 μ_B spin moment of the Co^{2+} ion (Table IX). The oxygen spin moments in both materials are comparable, and aligned in parallel to the cation spin moments on the octahedral sites. The width of the predominantly oxygen $2p$ valence band in $NiFe_2O_4$ is comparable to the one of $CoFe_2O_4$, but is reduced with respect to the valence band of magnetite. The reason being that the sixth localized d electron of the Fe^{2+} ion (in Fig. 2 (middle panel) seen at the bottom of the valence band between -5.0 and -6.0 eV) is strongly hybridized with the oxygen p band. The situation is different in $NiFe_2O_4$, where the three localized minority t_{2g} electrons, seen at about -8.0 eV (Fig. 4, bottom panel), are well separated from the bottom of the valence band. Also, the exchange splitting of the conduction band, of importance to spin filtering, is about 20% smaller in $NiFe_2O_4$ than in the Verwey phase of Fe_3O_4.

TABLE X: Spin decomposed exchange splittings of the valence and conduction bands, as well as the energy gaps (in eV), for both inverse and normal spinel structures for $NiFe_2O_4$. Here VBM stands for the valence band maximum and CBM for the conduction band minimum, and ↑ refers to spin-up- and ↓ to spin-down-component.

	'I' scenario	'N' scenario
$VBM^{\uparrow}$ - $VBM^{\downarrow}$	0.10	-0.12
$CBM^{\uparrow}$ - $CBM^{\downarrow}$	1.21	2.93
$CBM^{\uparrow}$ - $VBM^{\uparrow}$	2.19	3.31
$CBM^{\downarrow}$ - $VBM^{\downarrow}$	1.08	0.26
Gap	0.98	0.26

To understand details of the DOS of the 'I3+' scenario of $NiFe_2O_4$, it is helpful to follow the discussion of the same scenario for $CoFe_2O_4$, keeping in mind that a Ni^{3+} ion has two minority d electrons in addition to the five majority ones, localized by SIC. Obviously, as already mentioned when discussing $MnFe_2O_4$, the positions of the localized d peaks calculated in the SIC-LSD should not be directly compared with photoemission experiments.[40]

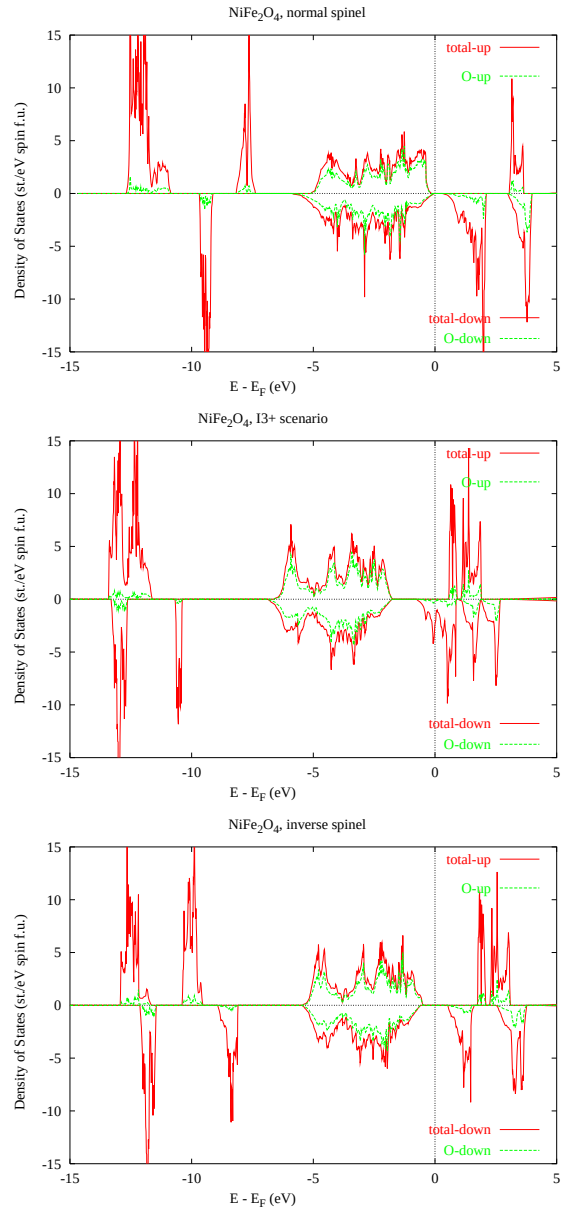

FIG. 4: (Color online) Spin decomposed total densities of states (in red), per formula unit, for $NiFe_2O_4$ in the normal spinel structure ('N') (top), $NiFe_2O_4$ in the inverse spinel structure for all 3+ ('I3+') scenario (middle), and $NiFe_2O_4$ in the inverse spinel structure ('I') (bottom). The oxygen contribution to the total density of states is also shown (green dotted lines). The minority DOS is printed on the negative side of the y-axis, while the majority contribution is shown on the positive side of this axis.

The changes in the electronic structure of $NiFe_2O_4$ when moving from the ground state inverse spinel structure to the normal spinel scenario are immediately obvious from comparing the bottom and top panels of Fig. 4. In the normal spinel case the Ni^{2+} ions occupy the tetra-

TABLE XI: Type-decomposed spin magnetic moments (in μ_B per formula unit), calculated within SIC-LSD, for $NiFe_2O_4$ for inverse and normal spinel scenarios. Here 'A' marks the tetrahedral-, while 'B1' and 'B2' the octahedral-sites, and 'O1' and 'O2' stand for two different types of oxygens.

Scenario	$Fe_A{}^{3+}$	$Ni_{B1}{}^{2+}$	$Fe_{B2}{}^{3+}$	O1	O2
I	-4.11	1.57	4.11	0.14	0.07
Scenario	$Ni_A{}^{2+}$	$Fe_{B1}{}^{3+}$	$Fe_{B2}{}^{3+}$	O1	O2
N	-1.65	4.13	4.13	0.35	0.35

hedral sites, while the octahedral sites are solely taken by the Fe^{3+} ions. As a result, the total spin magnetic moment is increased from 2 μ_B per formula unit to 8 μ_B per formula unit, as seen in Table II, in agreement with experimental findings of Refs. 11,12. However, as seen in the top panel of Fig. 4, the density of states is still just insulating in both spin channels. Also, unlike in the case of the inverse spinel structure, the valence band is strongly spin-polarized, and the polarization is negative. The oxygen spin magnetic moment is 0.35 μ_B, aligned in parallel to the Fe spin moment (see Table XI), and three times the value it has in the inverse spinel structure. Also, the Ni spin moment is slightly increased in magnitude to -1.65 μ_B. Moreover, the exchange splitting of the conduction band is more than twice increased in the normal spinel, in comparison with the inverse spinel structure, from 1.21 eV to 2.93 eV. As in the case of the other spinel ferrites in realizing Ni^{2+} ions, the e_g states are populated first, i. e., are lying lower in energy than the t_{2g} states, which is opposite to the inverse spinel structure. However, energetically, the normal spinel structure for $NiFe_2O_4$ is very unfavourable with respect to the inverse spinel structure (Table II).

Including the spin-orbit coupling for the ground state inverse spinel scenario gives rise to the total orbital moment of 0.67 μ_B per formula unit, and is mostly due to Ni ions, with some minor contributions from Fe atoms. This calculated value is over two times larger than calculated from LSD in Ref. 22. Also, in the earlier SIC-LSD calculations for TM oxides Svane and Gunnarsson[26] obtained the orbital moment for NiO of 0.27 μ_B, which is substantially smaller than in the present calculations. Since the total spin moment is slightly reduced to 1.9997 μ_B per formula unit, when SOC is taken into account, hence the ratio of the total orbital and spin moments is calculated to be about 0.34. The latter is in good agreement with the experimental estimates of 0.27±0.07[52] and 0.34 (within error bars of up to ±0.11) for Ni in $NiFe_2O_4$ and NiO.[52,53] Note that the orbital moment due to the Ni^{2+} ion alone is about 0.7 μ_B, while its spin moment is 1.58 μ_B, both per formula unit, giving rise to the orbital to spin moment ratio of 0.44 for this ion. The total orbital moment is mostly due to the Ni^{2+} ion, as the contributions of other TM ions are smaller by an order of magnitude or so.

V. CONCLUSIONS

We have shown that, owing to a better treatment of correlations, SIC-LSD can provide useful insights to the nature of a number of spinel ferromagnetic insulators. We have been able to address the issues of the normal versus inverse spinel arrangements in these systems, their electronic and magnetic properties and the valence of the transition metal atoms. We find all the studied ferrites to be insulating for both the inverse and normal spinel scenarios, with the calculated energy gaps being smaller in the normal spinel environment, however showing an increasing trend when moving from $MnFe_2O_4$ to $NiFe_2O_4$. We have observed dramatic increase of the calculated spin magnetic moments, as well as the exchange splitting of the conduction bands, when moving from the inverse to normal spinel scenarios, some of which have been observed in experiments.[11]

The total energy considerations seem to favour the inverse spinel arrangement of TM ions as the ground state configurations for all the studied ferrites, with the possible exception of $MnFe_2O_4$ where the normal spinel environment may be preferred, with Mn^{2+} ions on the tetrahedral sites and the Fe^{3+} ions on the octahedral sublattice. Also, based on the total energy arguments, we find a partial delocalization of the minority spin states to be favourable in Fe_3O_4 and $CoFe_2O_4$, leading to the half-metallic ground states with all TM ions in the trivalent configuration and in the inverse spinel arrangement. The fully inverse spinel scenario, with the Fe^{3+} ions on the tetrahedral sites and the octahedral sites occupied both by Ni^{2+} ions and Fe^{3+} ions, is found to be the ground state only in $NiFe_2O_4$. Finally, these findings constitute a good starting point for further studies, incorporating alloying of the normal and inverse spinel structures.

Acknowledgements

LP was supported by the Division of Materials Science an Engineering, Office of Basic Energy Sciences, US Department of Energy.

[1] I. Zutic, J. Fabian and S. Das Sarma, Rev. Mod. Phys. **76**, 323 (2004).

[2] J.M.D. Coey and M. Venkatesan, J. Appl. Phys. **91**, 8345 (2002).

[3] S. S. P. Parkin, C. Kaiser, A. Panchula, P. M. Rice, B . Hughes, M. Samant, and S.-H. Yang, Nat. Mater. **3**, 862 (2004).

[4] S. Yuasa, T. Nagahama, A. Fukushima, Y. Suzuki, and K.

Ando, Nat. Mater. **3**, 868 (2004).
[5] J. S. Moodera, X. Hao, G. A. Gibson, and R. Meservey, Phys. Rev. Lett. **61**, 637 (1988).
[6] P. LeClair, J.K. Ha, H.J.M. Swagten, C.H. van de Vin, J.T. Kohlhepp, and W.J.M. de Jonge, Appl. Phys. Lett. **80**, 625 (2002).
[7] V. A. M. Brabers, Handbook of Magnetic Materials, vol. 8 (1995).
[8] M. Pénicaud, B. Siberchicot, C. B. Sommers, J. Kübler, JMMM **103** 212 (1992).
[9] U. Lüders, M. Bibes, K. Bouzehouane, E. Jacquet, J.-P. Contour, S. Fusil, J.-F. Bobo, J. Fontcuberta, A. Barthélémy, and A. Fert, Appl. Phys. Lett. **88**, 082505 (2006).
[10] U. Lüders, A. Barthélémy, M. Bibes, K. Bouzehouane, S. Fusil, E. Jacquet, J.-P. Contour, J.-F. Bobo, J. Fontcuberta, and A. Fert, Adv. Mater. (in press); cond-mat/0508764.
[11] U. Lüders, M. Bibes, J.-F. Bobo, M. Cantoni, R. Bertacco, and J. Fontcuberta, Phys. Rev. B **71**, 134419 (2005).
[12] U. Lüders, G. Herranz, M. Bibes, K. Bouzehouane, E. Jacquet, J.-P. Contour, S. Fusil, J.-F. Bobo, J. Fontcuberta, A. Barthélémy, and A. Fert, J. Appl. Phys. **99**, 08K301 (2006).
[13] E.J.W. Verwey and P.W. Haayman, Physica (Utrecht) **8** (1941) 979; E.J.W. Verwey, P.W. Haayman and F.C. Romeijan, J. Chem. Phys. **15** 181 (1947).
[14] J.P. Wright, J.P. Attfield, and P.G. Radaelli, Phys. Rev. Lett. **87**, 266401 (2001).
[15] V. I. Anisimov, I. S. Elfimov, N. Hamada, and K. Terakura, Phys. Rev. B **54**, 4387 (1996).
[16] V. N. Antonov, B. N. Harmon, V. P. Antropov, A. Ya. Perlov, and A. N. Yaresko, Phys. Rev. B **64**, 134410 (2001).
[17] I. Leonov, A. N. Yaresko, V. N. Antonov, M. A. Korotin, and V. I. Anisimov, Phys. Rev. Lett. **93**, 146404 (2004).
[18] H.-T. Jeng, G. Y. Guo, and D. J. Huang, Phys. Rev. Lett. **93**, 156403 (2004).
[19] G. K. H. Madsen and P. Novak, Europhys. Lett. **69**, 777 (2005).
[20] Z. Szotek, W.M. Temmerman, A. Svane, L. Petit, G.M. Stocks and H. Winter, Phys. Rev. B **68**, 054415 (2003).
[21] H-T Jeng and G. Y. Guo, JMMM **239**, 88 (2002).
[22] H-T Jeng and G. Y. Guo, JMMM **240**, 436 (2002).
[23] D. J. Singh, M. Gupta, and R. Gupta, Phys. Rev. B **65**, 064432 (2002).
[24] X. Zuo and C. Vittoria, Phys. Rev. B **66**, 184420 (2002).
[25] W.M. Temmerman, A. Svane, Z. Szotek, and H. Winter, in *"Electronic Density Functional Theory: Recent Progress and New Directions"*, Eds. J.F. Dobson, G. Vignale, and M.P. Das (Plenum Press, New York and London, 1998).
[26] A. Svane and O. Gunnarsson, Phys. Rev. Lett. **65**, 1148 (1990).
[27] Z. Szotek, W.M. Temmerman, and H. Winter, Phys. Rev. B **47**, 4029 (1993).
[28] P. Strange, A. Svane, W.M. Temmerman, Z. Szotek and H. Winter, Nature **399**, 756 (1999).
[29] J.P. Perdew and A. Zunger, Phys. Rev. B**23**, 5048 (1981).
[30] O.K. Andersen, Phys. Rev. B**12**, 3060 (1975).
[31] O.K. Andersen and O. Jepsen, Phys. Rev. Lett. **53**, 2571 (1984).
[32] H.L. Skriver, The LMTO Method, Springer Series in Solid-State Sciences 41, Springer Verlag, 1984.
[33] J. M. Hastings and L. M. Corliss, Phys. Rev. **104**, 328 (1956).
[34] G. A. Sawatzky, F. van der Woude, and A. H. Morrish, Phys. Rev. **187**, 747 (1969).
[35] L. Braicovich, A. Tagliaferri, G. van der Laan, G. Ghiringhelli, and N. B. Brookes, Phys. Rev. Lett. **90**, 117401 (2003).
[36] W.R.L. Lambrecht and O.K. Andersen, Phys. Rev. B **34**, 2439 (1986).
[37] A. G. Flores, V. Raposo, L. Torres, and J. Iniguez, Phys. Rev. B **59**, 9447 (1999).
[38] A. J. Freeman, B. I. Min, and M. R. Norman, Handbook on the Physics and Chemistry of Rare Earths, eds. K. A. Gschneidner Jr., L. Eyring and S. Hüfner (North Holland, Amsterdam, Oxford, New York, Tokyo), 1987, Vol. 10, pp. 165-229.
[39] W. M. Temmerman, Z. Szotek, and H. Winter, Phys. Rev. B **47**, 1184 (1993).
[40] To improve the agreement between the calculated position of the TM d states from the SIC-LSD method and the photoemission measurement, one can perform Δ_{SCF} calculations, that is calculations of the total energy difference between two configurations of TM assumed to represent well the initial and final states of a photoemission experiment. This is expressed by the formula $\Delta_{SCF} = E(d^{n-1}, N_{val}+1) - E(d^n, N_{val})$, meaning that one removes an electron from a TM d level and introduces it at the top of the valence band, thus increasing the total number of valence electrons, N_{val}, by 1. Here E represents the total energies of the respective d^{n-1} and d^n configurations. Of course, a problem one faces with this kind of estimate is that the correct final state might not be the ground state of the system with one electron removed.
Another way of improving the agreement with spectroscopies is to apply the OEP philosophy. The SIC-LSD method is an orbital dependent density functional theory. Formally, however, SIC-LSD may be viewed as a standard density functional theory, implying that the SIC-LSD energy functional can be represented as a functional of the total charge density alone and minimized with respect to it. This means that there exists an effective Kohn-Sham equation with an effective potential, which is common to all Kohn-Sham states, is self-interaction free and depends only on the total charge density. Here the situation is completely analogous to the optimized effective potential introduced in connection with the Hatre-Fock approximation,[41,42] for which case the Kohn-Sham eigenvalues are often compared to quasiparticle energies, with a considerable improvement over the Hartree-Fock eigenenergies. Adopting the OEP philosophy, one can search for the effective potential, which reproduces the SIC spin-density, and with such a potential derive the density of the localized TM d states. The search may be constrained by looking only for that particular potential shift on the TM sites, which will reproduce the self-consistent TM spin moment of the SIC-LSD calculations.
[41] J. B. Krieger, Y. Li, and G. J. Iafrate, Phys. Rev. A **45**, 101 (1992); J. B. Krieger, Y. Li, and G. J. Iafrate, Phys. Rev. A **46**, 5453 (1992); Y. Li, J. B. Krieger, and G. J. Iafrate, Phys. Rev. A **47**, 165 (1993).
[42] T. Kotani, J. Phys.: Condens. Matter **10**, 9241 (1998).
[43] R. T. Sharp and G. K. Horton, Phys. Rev. **90**, 317 (1953).
[44] J. D. Talman and W. F. Shadwick, Phys. Rev. A **14**, 36 (1976).
[45] M. R. Norman and D. D. Koelling, Phys. Rev. B **30**, 5530 (1984).
[46] F. Walz, J. Phys.: Condens. Matter **14** (2002) R285.

[47] S.K. Park, T. Ishikawa, and Y. Tokura, Phys. Rev. B **58**, 3717 (1998).

[48] Note that our SIC-LSD calculations for the Verwey scenario and the true low temperature monoclinic phase obtained a gap of ∼0.1 eV,[20] which compares well with the experimental value of 0.14 eV[47].

[49] R. A. D. Pattrick, G. van der Laan, C. M. B. Henderson, P. Kuiper, E. Dudzik, and D. J. Vaughan, Eur. J. Mineral. **14**, 1095 (2002).

[50] Y. Waseda, K. Shinoda, and K. Sugiyama, Z. Naturforsch. **50a**, 1199 (1995).

[51] H. St.-C. O'Neill and A. Navrotsky, Am. Mineral. **68**, 181 (1983).

[52] G. van der Laan, C. M. B. Henderson, R. A. D. Pattrick, S. S. Dhesi, P. F. Schofield, E. Dudzik, and D. J. Vaughan, Phys. Rev. B **59**, 4314 (1999).

[53] V. Fernandez, C. Vettier, F. de Bergevin, C. Giles, and W. Neubeck, Phys. Rev. B **57**, 7870 (1998).